
# Brain Cortical Surface Registration with Anatomical Atlas Constraints

Wei Zeng[1(✉)], Xuebin Chang[1], Liqun Yang[2], Muhammad Razib[3], Zhong-Lin Lu[4], and Yi-Jun Yang[1]

[1] Xi'an Jiaotong University, Xi'an, China
wz@xjtu.edu.cn
[2] China Nanhu Academy of Electronics and Information Technology, Jiaxing, China
[3] Florida International University, Miami, FL, USA
[4] New York University, New York, NY, USA

**Abstract.** This work presents a novel cortical surface registration framework by using the whole anatomical atlas structures as correspondence constraints, which are extracted as atlas graphs (nodes are the junctions and edges are the intersecting curves of regions). The focus of this work is on the geometric registration category of cortical surfaces, i.e., brains are registered only using structural information without any functional information. We aim to innovate the geometric registration framework by utilizing the prominent anatomical features, atlas, to drive the registration. Intuitively, we convert the 3D cortical surfaces to 2D disks by special geometric mappings, where the curvy atlas regions become straight and convex polygonal regions; then registration is achieved between 2D domains such that curvy constrains become linear constraints and are solvable in linear time. The mappings generated are intrinsic and have theoretic guarantee of existence, uniqueness and optimality in terms of constrained harmonic energy. It differs from the literature geometric approaches using brain curves or point features. To the best of our knowledge, it is the first work of using atlas graph constraints in geometric registration. Our experiments on various brain data sets demonstrate the efficiency and efficacy for brain registration and the practicability of the proposed framework for brain disease classification.

**Keywords:** Surface registration · anatomical altas · geometric approaches · graph constraints

## 1 Introduction

Medical image registration has been widely used in image-guided interventions, patient response to treatment, and morphometric analysis. Cortical registration is important since the role of the cerebral cortex in higher-order cognitive function [2]. To ensure the accuracy of surface alignment, landmarks representing distinctive features of the surface are often used to guide the alignment, e.g. curves or points.

There have been a lot of researches on cortical geometric registration (see [3] for a survey). Existing geometric registration methods usually use sulci curves or points as constraints. The challenge is how to guarantee diffeomorphism under these constraints.


G. Bebis et al. (Eds.): ISVC 2023, LNCS 14361, pp. 357–369, 2023.
https://doi.org/10.1007/978-3-031-47969-4_28

1) Point-constrained methods. Some progresses have been made recently toward solving that. The geodesic flows [12] generate diffeomorphisms along the deformation process. The hyperbolic orbifold model [22] guarantee a diffeomorphism with the exact landmark point alignment. 2) Curve-constrained methods. Most works discretize curves to points [4], but cannot guarantee the alignment of point intervals. Rigorous methods to handle curve constraints have been presented based on the hyperbolic harmonic map [19] and the quasiconformal map [24].

Moreover, the atlas graph's intrinsic curvature and pronounced non-linearity present substantial hurdles when striving for diffeomorphic registration. Taking inspiration from Tutte graph embedding, a technique ensuring convexity for each graph face, we introduce an intrinsic method for convex subdivision mapping applied to 3D surfaces. This novel approach facilitates atlas-based registration while circumventing the need for graph embedding, effectively transforming the 3D curvilinear graph constraints into linear straight-line constraints.

In summary, we present a novel cortical geometric registration framework using anatomical atlas structure as constraints. The major contributions of the proposed brain registration method are as follows:

1. The registration based on intrinsic convex subdivision harmonic map respects intrinsic surface and landmark geometry. It exists and is globally optimal, unique and diffeomorphic. Importantly, the registration achieves more accuracy.
2. The proposed registration with consistent feature graphs (if not consistent, then the graphs are made consistent with graph refinement strategy) has been proved to be globally optimal, unique and diffeomorphic.

Additionally, we have two strategies to validate that: (1) We evaluated the accuracy of the proposed registration by the comparison to the results using only common atlas graphs (without atlas refinement) and FreeSurfer results. (2) We then applied the shape metrics obtained from the registration to the brain classification between Alzheimer's disease (AD) group and healthy control (CTL) group. The classification accuracy is 88% with our method which is better than that using Freesurfer registration [5].

## 2 Approach Overview

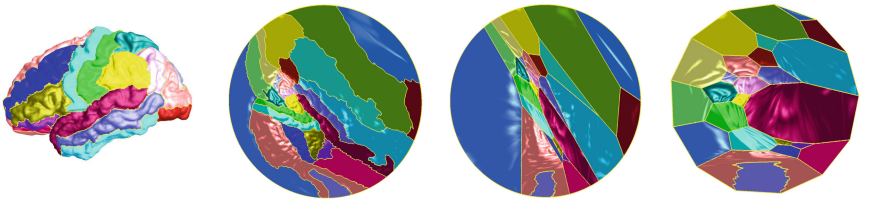

(a) 3D brain (b) harmonic map (c) our mapping (d) uniform mapping

**Fig. 1.** Cortical surface mappings, where atlas regions are color encoded.

The overall solution is based on the proposed intrinsic graph-driven harmonic map along with graph modification and mapping relaxation techniques. Without considering

graph constraint, the harmonic map is intrinsic, but the graph appears highly curvy on the planar domain (see Fig. 1a–b), which cannot be used directly as constraint. In our intrinsic convex harmonic map, boundary vertices are prescribed onto the unit circle using arc length weight, the positions of mesh vertices on atlas graph (including graph nodes) are automatically computed using the weight on their adjacent mesh edges on graph, and the positions of other interior mesh vertices are computed automatically. This setting ensures that the atlas graph is straightened to be convex (see Fig. 1c). The positions computed is intrinsically determined by the surface and graph geometry. In contrast, in the uniform convex mapping [14] (see Fig. 1d), the positions of the graph nodes are given by the uniform Tutte embedding, which are not intrinsic without considering graph geometry.

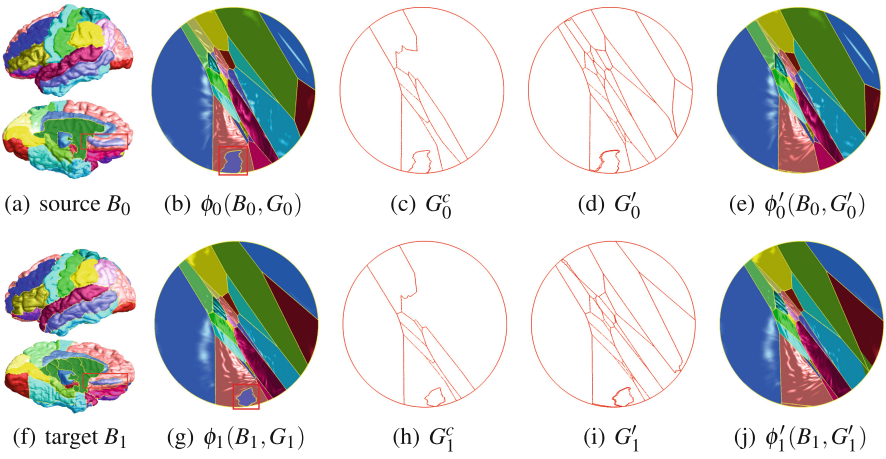


**Fig. 2.** The pipeline of the registration for cortical surfaces. (a)–(e) represents the processing of a convex graph based on cerebral cortex $B_0$ from the original graph $G_0$ to the refined graph $G_0'$; (f)–(g) represents the processing of a convex graph based on cerebral cortex $B_1$ from the original graph $G_1$ to the refined graph $G_1'$. $G_k^c$: maximal common subgraphs, $G_k'$: consistent refined graphs (red rectangles highlights two-edged regions), $\phi_k$: convex map with original graph, $\phi_k'$: convex map with refined graph and $k = 0, 1$. (Color figure online)

Given the source and target cortical surfaces to be registered, *first*, we check the atlas graph consistency and perform minimal changes to make graphs 3-connected (i.e., node degree $\geq 3$, required in convex embedding [7]) and isomorphic. *Then*, we construct the registration over the intrinsic convex subdivision domains by a harmonic map constrained with the linear convex subdivision constraint. *Finally*, we perform a relaxation process to minimize the distortions introduced by graph modification. The resulted registration is guaranteed to be unique and diffeomorphic based on the generalized Radó theorem [17] and Floater's convex combination theorem [7]. The method is linear, implemented by solving sparse linear systems. Figure 2 illustrates the pipeline of the registration for cortical surfaces $B_0, B_1$. The atlas graphs are inconsistent, but with common subgraphs. The graphs are locally modified around unmatched edges and two-edged regions (as shown in the red rectangles). We can observe that the two-edged

regions become three-edged regions and the graphs are mapped to convex subdivisions. In the graph-driven harmonic mapping method, the weights are specially set for the triangle edges on the atlas graph curves, so that the result respects the geometry intrinsically and is proven to be a diffeomorphism based on the Floater's convex combination theorem [7]. Experiments were performed on Mindboggle [10] and LPBA40 [18] and data sets with manual atlas labels to verify atlas inconsistency and to evaluate the algorithm performance.

## 3 Computational Algorithms

The major steps for registration include: 1) check atlas consistency and refine atlas graph if inconsistent; 2) compute intrinsic atlas-constrained harmonic maps; and 3) register the two harmonic map domains and relax the mapping due to atlas modification.

The cortical surface is represented as a triangular mesh of genus zero with a single boundary (the back-side unknown region is cut off), denoted as $M = (V, E, F)$, where $V, E, F$ represent vertex, edge and face sets, respectively. The atlas graph is denoted as $G = (V_G, E_G, F_G, V_{E_G})$, where $V_G, E_G, F_G$ represent graph node, edge and face sets, respectively, and $V_{E_G}$ represents all mesh vertices on graph. Here a graph edge is formed by a chain of vertices. We use $(M, G)$ to denote an atlas-constrained surface.

Given two surfaces $(M_1, G_1)$, $(M_2, G_2)$, the goal is to find an optimal diffeomorphism $f : (M_1, G_1) \to (M_2, G_2)$, such that atlases $G_1$ and $G_2$ are aligned as constraint. If $G_1, G_2$ are not consistent, we modify them as little as possible to be consistent, i.e., $G_1' \sim G_2'$. The registration employs the 3D-to-2D strategy, which maps 3D surfaces to 2D canonical domains and then simplifies 3D surface registration problems to 2D ones. We first compute the intrinsic graph-driven harmonic maps $\phi_k : (M_k, G_k') \to (D_k, \hat{G}_k')$, where $G_k'$ are canonicalized to be planar convex subdivisions $\hat{G}_k'$ on the unit disk $D_k$. Then we compute the mapping $h : (D_1, \hat{G}_1') \to (D_2, \hat{G}_2')$ via a constrained harmonic map, followed by an operation $\eta$ to relax the distortions introduced by atlas modification. Therefore, the registration $f = \phi_2^{-1} \circ \eta \circ h \circ \phi_1$, as shown in Diagram (3). For simplicity, due to the property of convex harmonic map, the registration can also be computed as:

$$\begin{array}{ccc} (M_1, G_1) & \xrightarrow{f} & (M_2, G_2) \\ \phi_1 \downarrow & & \downarrow \phi_2 \\ (D_1, \hat{G}_1) & \xrightarrow{h} & (D_2, \hat{G}_2) \end{array} \tag{3}$$

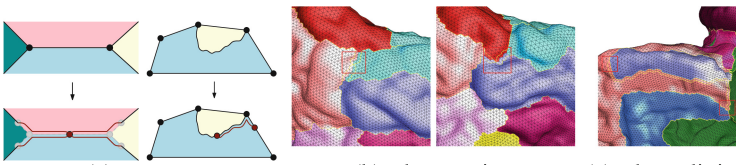

(a) strategy (b) edge pruning (c) edge splitting

**Fig. 3.** Atlas refinement: illustration (a) and examples of edge pruning (b, source vs. target) and edge splitting (c).

### 3.1 Atlas Consistency Check and Refinement

We first check whether the two atlas graphs are consistent or not. Two nodes are matched (consistent) if they have exactly the same surrounding regions. If all nodes are matched, then $G_1 \sim G_2$. Otherwise, we perform refinement operations (see Fig. 3a), as follows:

1. Refine unmatched edges by edge pruning (see Fig. 3b). Two graph edges in both atlases are matched, if they have the same left and right neighboring regions. We remove the unmatched edge by moving two nodes to the middle. The original graph edge is then divided into two segments. Each segment is shifted to every side by one triangle away from the original position. Repeat edge pruning until there is no unmatched edge. This operation won't introduce new connectivity between regions.
2. Refine two-edged regions by edge splitting. These regions have only two graph nodes and edges (see Fig. 2a,b,f,g, Fig. 3c), and need to be refined as 3-connected (degree $\geq 3$), required in convex embedding. We first split the interior edge at the middle vertex to segments and then perturb one segment by one triangle away from the original. Thus the region becomes three sided. The selections of the interior edge for splitting and the segment for perturbing are remembered for consistent operation over atlases.

### 3.2 Intrinsic Graph-Driven Harmonic Map

We map the cortical surface $M$ onto the convex subdivision domain $D$, $\phi : (M, G') \rightarrow (D, \hat{G}')$, by minimizing harmonic energy (stretches) with the atlas graph conditions. The critical point of harmonic energy is a harmonic map. The energy is formulated as

$$\min\{E(\phi(v_i)) = \Sigma_{[v_i,v_j]\in E} w_{ij}(\phi(v_i) - \phi(v_j))^2, \forall v_i \in V\}, \tag{1}$$

where $w_{ij}$ is the edge weight; in our method, we use the mean value coordinates [14] as edge weights.

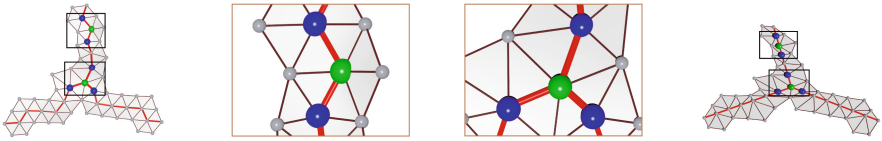

(a) graph edge, graph node (b) zoomed view of graph edge (c) zoomed view of graph node (d) intrinsic map

**Fig. 4.** Adaptive mean value coordinate. (a) shows graph edge on the top box and graph node on the bottom box, (b) and (c) show the zoomed in view of graph edge and graph node. The blue points are the *one-ring graph neighborhood* of the green ones. (Color figure online)

We map the outer boundary of the brain surface to the unit circle. We employ special handling to automatically and intrinsically map the curvy graph $G'$ as a convex subdivision on the unit disk. To achieve this without graph embedding, we modify the mean

value coordinate adaptively according to the atlas graph such that the convex combination map defined in Eq. (1) satisfies the Circumferential Mean Value Theorem [6] at every interior vertex, and it straightens the feature graph to the convex subdivision. In detail, for a vertex on the atlas graph, we define its *one-ring graph neighborhood* as its adjacent vertices lying on the graph (see Fig. 4). For the vertices on the feature graph, we utilize their one-ring graph neighborhood during the computation of the adaptive mean value coordinate, and the interior points of the graph curves will move to the linear interpolation of their two adjacent graph neighbors on the feature curves instead, which will result in a convex subdivision in the canonical domain (see Fig. 2e, j). In detail, to compute the intrinsic harmonic map of graph constrained surfaces, we compute the harmonic weights adaptively as follows (see Fig. 4). If the vertex $v_0$ is

1. not on the graph, then we utilize the mean value coordinate as the weight.
2. lying inside the interior of graph edge, then the barycentric coordinate is applied to its one-ring graph neighborhood instead. Let $v_1$ and $v_2$ denote its two adjacent neighboring vertices on the graph. The adaptive harmonic weight is defined as $w_1 = \frac{|v_2-v_0|}{|v_2-v_0|+|v_1-v_0|}$ and $w_2 = \frac{|v_1-v_0|}{|v_2-v_0|+|v_1-v_0|}$.
3. the graph node, then the Circumferential Mean Value Theorem is applied to its one-ring graph neighborhood to compute the adaptive harmonic weight.

In our construction, each vertex of the surface is a convex combination of neighbors. The resulted mapping is guaranteed to be unique and diffeomorphic and a convex subdivision based on Radó theorem [17] and Floater's convex combination theorem [7].

### 3.3 Diffeomorphic Graph-Constrained Registration

With the refined consistent atlas graphs, the source $(M_1, G_1')$ and target $(M_2, G_2')$ are mapped onto the disk domains with interior convex subdivision by the above intrinsic harmonic map. We then register the two planar domains, $h : (D_1, \hat{G}_1') \to (D_2, \hat{G}_2')$, by minimizing the harmonic energy. We specify the positions of the boundary vertices (by interpolation) and the graph nodes as the corresponding ones on the target, and set the combinations for the vertices on graph edge only using adjacent edges on graph. The resulted mapping is diffeomorphic.

The virtual curve by atlas refinement may introduce fake alignment. Thus we relax the mapping $h$ to lower the distortions.

We first set $\eta = h$. At each step, we compute the gradient of vertex $v_i \in V_1$, $\triangle\eta(v_i) = \sum_{[v_i,v_j]\in E} w_{ij}(\eta(v_i) - \eta(v_j))$, and update $\eta(v_i) \leftarrow \eta(v_i) - \lambda(v_i)d\eta(v_i)$, where $\lambda \in [0,1]$ is a movement scalar function. In detail, (1) for the graph nodes which are on both original and refined graphs of $M_1$ and boundary vertices, we set $\lambda = 0$ (i.e., exactly aligned by $h$ and fixed); (2) for the vertices which are on virtual curves, we set $\lambda = 1$. To further smoothen the mapping at the end areas of virtual curves, we set $\lambda = \frac{d}{r}$ for the vertices inside, where $d$ is the distance to endpoint, $r$ is the radius of the range; and (3) for the resting mesh vertices, we set $\lambda = 1$ (i.e., with full movement).

The size of local range needs to be carefully selected, depending on the length of the virtual curve. We have flipping check during the relaxation procedure, and reduce movement scalar or stop moving if the movement produces flip. In this relaxation, each

**Table 1.** Statistics on atlas graphs: $G$ - original graph, $G^c$ - maximum common subgraph, and $G'$ - refined consistent graph over all brains.

| Data (left hemisphere) | $G$-#v/e/f | $G^c$-#v/e/f | $G'$-#v/e/f | #unmatched e | #two-edged f | #triangle, time |
|---|---|---|---|---|---|---|
| Mindboggle | 59–71/89–103/31 | 0/0/0 | 25/47/23 | 25.10 | 0 | 293$k$, 50 s |
| LPBA40 | 46–48/68–72/25 | 0/0/0 | 19/40/22 | 25.85 | 1.175 | 131$k$, 20 s |

step reduces the constrained harmonic energy, and therefore this iterative process converges. The composed mapping $\eta \circ h$ gives a diffeomorphism. Along with the $\phi_k$, we can generate the diffeomorphic registration $f$ between the 3D atlas-constrained cortical surfaces, under the optimality criterion of minimizing stretches.

## 4 Experiments

The proposed algorithms underwent validation using publicly available human brain datasets that included manual atlas labels. Specifically, we used a dataset comprising 40 brains from LPBA40 [18] (processed through BrainSuite) and another dataset containing 95 brains from Mindboggle [10]. Notably, these two databases adhere to different protocols for human cortical labeling, resulting in the creation of distinct atlases. Therefore, we conducted registration independently within each database.

To further assess the effectiveness of our method, we applied it to the Alzheimer's Disease Neuroimaging Initiative (ADNI) dataset [9] for Alzheimer's disease classification. All experiments were conducted on a workstation equipped with a 3.7GHz CPU and 16GB of RAM. Our algorithm was implemented in C++, with Matlab serving as the solver for sparse linear systems. It's worth noting that all computations were executed automatically, ensuring stability and robustness without the need for manual intervention.

### 4.1 Atlas Consistency Analysis and Refinement

Under the same labeling protocol, brains have consistent cortical regions, but no consideration on the junctions (graph nodes) of anatomical regions among brains.

We have done the statistics on the two data sets, as follows: (1) all atlas graphs are embedded on the hemispherical cortical surfaces and are intrinsically planar; (2) LBPA40 data has at most 2 two-edged regions, violating "3-connected" property, and Mindboggle data has no; and (3) atlas graphs are not consistent (isomorphic) among brains, and there is no common subgraphs in each data set, therefore the connection types at junctions are diverse. Furthermore, by comparing the number of triangle edges of unmatched graph edges over brains, the differences of atlas graphs are restricted to a local range (less than 10 in most cases). By graph refinement, the original regions won't disappear. For example, in Fig. 2, the consistent refined graph for brain pair $(B_0, B_1)$ has 45 nodes, 70 edges, and 26 faces (same as the original). Table 1 gives the statistics for all brains in each data set.

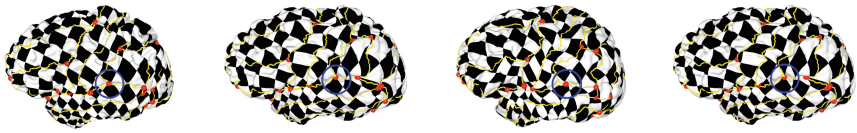

(a) source $B_0$ (b) target $B_1$ (c) target $B_2$ (d) target $B_3$

**Fig. 5.** Registration **I** by refining atlases for each pair $<B_0, B_k>, k = 1,2,3$ separately.

### 4.2 Atlas-Based Brain Registration

We applied our registration framework within each data set. Table 1 gives the averaged running time for registering one pair of cortical surfaces. The computational algorithm is efficient and practical. In each data set, we select a brain $B_0$ (as a reference) to register every other brain, to achieve the co-registration among all brains. Here, for illustration, we show four brains' registration results, $(B_0, G_0), (B_1, G_1), (B_2, G_2), (B_3, G_3)$. Two ways of atlas refinement are as follows: **I.** Refine atlases to be consistent for each pair separately. **II.** Refine atlases to be consistent for 4 brains together. We found out the unmatched edges among all atlases and prune them iteratively. Figures 5 and 6 show the registration results, respectively.

By the registration, we transferred the texture coordinates (e.g., using disk harmonic map parameters in Fig. 1b) of $B_0$ to all other brains, then the one-to-one registrations can be visualized by the consistent texture mappings (see blue circle areas in Fig. 5). Numerically, we computed the registration accuracy metric as the *dice coefficient* to measure the overlap between regions of $M_k^i$, defined as $D_c(M_1, M_2) = 2 * \frac{\sum_i A(M_1^i \cap M_2^i)}{A(M_1) + A(M_2)}$,

where $A$ is the area function. The larger value indicates more accuracy. We performed the following experiments to evaluate the accuracy of the proposed registration method:

For the pair $(B_0, B_1)$, we evaluated the performance under two cases of graph constraints: 1) the maximum common subgraph, and 2) the consistent refined graphs, with the registration accuracy $D_c = 0.88324, 0.9589$ (without relaxation), respectively. This shows that the refined graph registration performs better and verifies the intuition. We tested different smoothness levels in relaxation by selecting 1-ring (no interior vertices, no control on smoothness), 2-ring and 3-ring local ranges, with $D_c = 0.9590, 0.9589, 0.9589$, respectively. The results are similar, but the 1-ring gives the highest result due to less restriction to the movement. Registration with relaxation shows better results than the initial one. We chose 2-ring one to balance smoothness and accuracy.

We made comparisons with the FreeSurfer registration [5], which is computed by running the FreeSurfer software using the parameter "Mri_cvs_register". We have done the evaluation on both registration accuracy and efficiency on three databases including Mindboggle (95 brains), LPBA40 (40 brains), and ADNI (100 brains). The Dice measure on the registration results [23] showed our method performs better than FreeSurfer. With the curvature metric [16], our tests show that our method has 9% higher accuracy on average. In addition, our method is computed by solving sparse linear systems

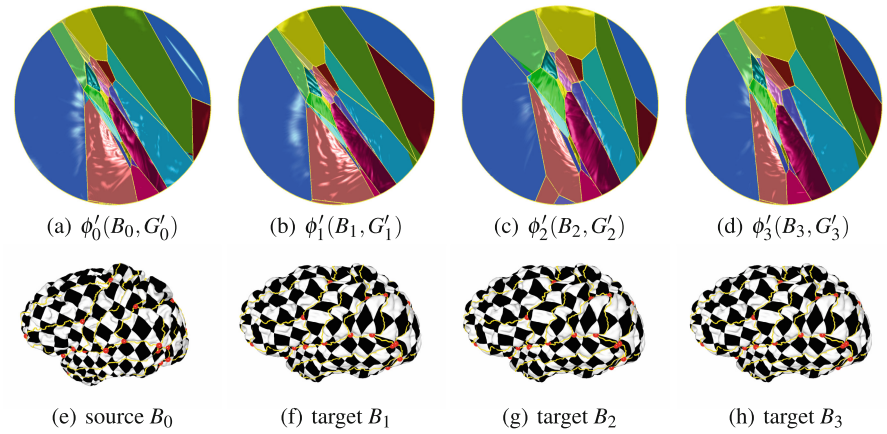

(a) $\phi_0'(B_0, G_0')$ (b) $\phi_1'(B_1, G_1')$ (c) $\phi_2'(B_2, G_2')$ (d) $\phi_3'(B_3, G_3')$

(e) source $B_0$ (f) target $B_1$ (g) target $B_2$ (h) target $B_3$

**Fig. 6.** Registration **II** by refining atlas for multiple brains together. Top: the intrinsic harmonic maps with consistent refined graphs, $\phi_i' : (B_i, G_i') \to (D_i, \hat{G}_i'), i = 0, 1, 2, 3$. Row 2: the one-to-one registration visualized by consistent texture mappings.

and is more efficient and much faster than the nonlinear FreeSurfer method [5], which has been verified in the practical experiments. As an illustration, for the three pairs $(B_0, B_k), k = 1, 2, 3$, we compared the registration results under the two graph refinement strategies **I**, **II** with the FreeSurfer results [15]. The registration accuracy $D_c$ (FreeSurfer, **I**, **II**) is (0.8123, 0.9589, 0.9595) for $(B_0, B_1)$, (0.8825, 0.9611, 0.9560) for $(B_0, B_2)$, and (0.8838, 0.9628, 0.9612) for $(B_0, B_3)$. Our method has higher accuracy.

### 4.3 Application to AD Classification

Accordingly, the proposed registration framework also produces more accurate shape metrics, which is evaluated by the efficiency of using the obtained shape metrics to classify brains with neudegenerative disease, e.g., AD. The criterion is the classification accuracy. To perform this, we applied the proposed registration method on ADNI data set to classify AD patients, and compared that with FreeSurfer shape metric for the same data.

**Participants.** Structural brain magnetic resonance imaging (MRI) scans were obtained from ADNI database (adni.loni.usc.edu). For up-to-date information, see www.adni-info.org. A total of 100 brains with 50 age-matched AD brains and 50 CTL brains (Age: AD: 56.5–86.7, CTL: 59.9–89.6; Mini-Mental State Examination score: AD: 20–27, CTL: 26–30) were considered in this study. The cross-sectional study was approved by the Local Ethical Committee on human studies and written informed consent from subjects was obtained prior to their enrolment.

**Data Processing.** All the brains were processed by Freesurfer's (version 5.1) automated pipeline using the command *recon-all* with default parameters to generate parcellated surfaces. For registration, we randomly select one brain as the source, and register that to all other 99 brains. After the registration, all the brains have one-to-one vertex correspondence. Consider that cortical atrophy is a valid biomarker of AD-related neurode-

generation. We used a total of 17 attributes for each vertex. The attributes are, (1) area on the pial surface, (2) area on the mid cortical surface, (3) gaussian curvature on the white surface, (4) gaussian curvature on the pial surface, (5) average curvature on the white surface, (6) sulcul depth on the white surface, (7) cortical thickness on the white surface, (8) cortical volume on the white surface, (9) bending energy (BE) on smooth white matter surface (smoothwm), (10) curvedness (C) on smoothwm, (11) folding index (FI ) on smoothwm, (12) mean curvature (H) on smoothwm, (13) gaussian curvature (K) on smoothwm, (14) maximum curvature ($K_1$) on smoothwm, (15) minimum curvature ($K_2$) on smoothwm, (16) sharpness (S) on smoothwm, and (17) atlas region. Mean curvature, H is defined as $1/2 \times (K_1 + K_2)$; Gaussian curvature, K is defined as $K_1 \times K_2$; Curvedness, C is defined as, $\sqrt{\frac{K_1^2 + K_2^2}{2}}$; bending energy, BE is defined as $K_1^2 + K_2^2$; folding index, FI is defined as $|K_1| \times (|K_1| - |K_2|)$ [13]. The attributes are interpolated from the target to the deformed surfaces using the correspondence from the registration process. Most current AD classifications only mention indicators such as cortical curvature and volume without detailed feature extraction from the cerebral cortex, and we also believe that refined brain features are more reflective of changes in the cerebral cortex, thus providing a reference for diagnosis.

We computed the distance between the source and the deformed source (registered to target) for all the 17 attributes for each region (total 35 regions excluding the black/unknown region, as obtained by Freesurfer) and used those as the features for the classification. For the attribute region, we assign 0 for the similarity and 1 otherwise; for all other attributes we used the Euclidean distance. Therefore, we get a total of $35 \times 17 = 595$ features for the 35 regions. To detect the important features for classification, we used forward sequential feature selection algorithm [11], and selected a total of 200 features out of these 595 features. After that, we searched over the 200 features incrementally to identify the best combination of features for the classification.

**Classification.** We used two classification algorithms, (1) Support Vector Machine (SVM) and (2) K Nearest Neighbor (K-NN), with 10-fold cross validation. We used Matlab implementation of both the algorithms. For the SVM algorithm, Gaussian radial basis kernel function (rbf) was used with a scaling factor of 3.63 and box constraint of 2.71. The optimal scaling factor and box constraint were obtained by using the bayesian hyper parameters optimization [21] process. For K-NN algorithm, we used K = 5. We searched incrementally over the features for both SVM and K-NN (see Fig. 7a). The classification accuracy for SVM is 86.0% with false positive rate (FPR) = 8.0% and false negative rate (FNR) = 20.0%, and accuracy for K-NN is 88.0% with FPR = 6.0% and FNR = 18.0% (see Table 2). Both algorithms achieved the best accuracy with 98 features. To visualize the trade-off between the true positive rate (TPR) and FNR, we used Receiver Operating Characteristic (ROC). Figure 7b shows the ROC curve for SVM and K-NN; area under curve (AUC) value for SVM is 0.856, and for K-NN is 0.882.

**Table 2.** AD classification accuracy with SVM and K-NN.

| Algorithms | Sensitivity | Specificity | AUC | Accuary (Ours) | Accuary (FreeSurfer) |
|---|---|---|---|---|---|
| SVM | 92.0% | 80.0% | 0.856 | 86.0% | 82.0% |
| K-NN | 94.0% | 82.0% | 0.882 | 88.0% | 78.0% |

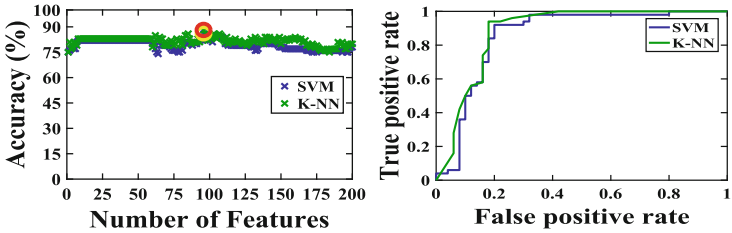


(a) feature selection (b) ROC curve

**Fig. 7.** Classification. (a) The accuracy using different number of features obtained by FSFS algorithm for SVM and K-NN. (b) The ROC curve for SVM and K-NN.

We evaluated our method with the shape metrics with FreeSurfer's registration method. We used the same setting for both SVM and K-NN, and used the same number of features with same number of anatomical atlas regions (excluding the black/unknown region as before). Using the same 98 features, classification accuracy using FreeSurfer registration is 82.0% with SVM, and 78.0% with K-NN (see Table 2). For both algorithms, our registration results perform better as they provide more accurate alignment of the corresponding atlas regions with similar shapes in the registration process and accordingly more accurate shape metrics among them.

## 5 Discussion

The proposed registration method achieves a delicate equilibrium by aligning atlases to their fullest extent while simultaneously minimizing harmonic energy, thereby preserving local shapes within defined constraints. It is crucial to acknowledge that achieving a flawless registration for cortical surfaces characterized by inherently inconsistent atlases is a formidable challenge. Our approach is meticulously designed to confine alterations primarily to local regions.

Our methodology introduces one-triangle-wide pieces, the smallest units within a triangular mesh, which serve to significantly reduce distortions from the original atlas. This innovative technique preserves the original atlas geometry on the cortical surface to an impressive degree. Additionally, the relaxation procedure further mitigates these distortions. Notably, our method is renowned for its rigor, intrinsic nature, and linearity, as it leverages the classical harmonic map with convex subdivision constraints, offering assurances of uniqueness and diffeomorphism [7].

What truly sets our work apart is our pioneering use of entire cortical atlases as constraints, intrinsically mapping cortical surfaces with atlas graphs onto a convex subdivision domain. Moreover, we have harnessed mean value coordinates to align regions of interest within the cerebral cortex, streamlining the process of atlas alignment across diverse brains. We emphasize that public databases like Mindboggle and LPBA40 predominantly provide structural MRI data paired with manually labeled atlases. Our geometric registration methodology's shape representations and metrics can be seamlessly integrated with fMRI or dMRI data, forming the foundation for a comprehensive multimodal cortical surface registration framework. To guide this integration, we plan to

follow the established pipeline proposed in the Multimodal Surface Matching works [16], systematically evaluating the fusion of multiple data modalities.

Our future initiatives entail the incorporation of functional information into our framework, thus enriching our registration approach for a more comprehensive biological interpretation in diverse brain applications. Additionally, we will conduct comparative analyses with CAT12 [8] and ANTs [1], using the same dataset, further expanding the scope of our research.

Within this overarching framework, we anticipate the exploration of more sophisticated methodologies, such as bijective maps designed to minimize distortion metrics without confining graph boundaries to fixed shapes [20]. Furthermore, we aim to incorporate optimization criteria, including minimizing angle or area distortions, to further enhance our registration capabilities.

## 6 Conclusion

This work presents a novel geometric method to register cortical surfaces with structural atlas constraints. We first perform atlas consistency check and refinement, then convert surfaces to 2D convex subdivision domains by the intrinsic graph-driven harmonic maps, and finally compute the registration over the 2D domains, followed by a relaxation procedure. The mapping is unique and diffeomorphic. The whole process is automatic. Experiments on co-registering brains in two public databases, and the application to Alzheimer's Disease classification have demonstrated the efficiency and practicality of the algorithms. We will further explore the proposed framework by integrating multimodal information and apply that to large-scale brain morphometry analysis and medical and cognitive problems in future works.

**Acknowledgment.** This work was supported by National Key R&D Program of China (Grant No. 2021YFA1003002) and NSFC (Grant No. 12090021). Data collection and sharing for this project was funded by the Alzheimer's Disease Neuroimaging Initiative (ADNI) (National Institutes of Health Grant U01 AG024904) and DOD ADNI (Department of Defense award number W81XWH-12-2-0012).

## References

1. Avants, B.B., Tustison, N., Song, G., et al.: Advanced normalization tools (ANTs). Insight J. **2**(365), 1–35 (2009)
2. Che, T., et al.: AMNet: adaptive multi-level network for deformable registration of 3D brain MR images. Med. Image Anal. **85**, 102740 (2023)
3. Cheng, J., Dalca, A.V., Fischl, B., Zöllei, L., Initiative, A.D.N., et al.: Cortical surface registration using unsupervised learning. Neuroimage **221**, 117161 (2020)
4. Choi, P.T., Lam, K.C., Lui, L.M.: FLASH: fast landmark aligned spherical harmonic parameterization for genus-0 closed brain surfaces. SIAM J. Imaging Sci. **8**(1), 67–94 (2015)
5. Fischl, B., Sereno, M., Dale, A.: Cortical surface-based analysis II: inflation, flattening, and a surface-based coordinate system. Neuroimage **9**(2), 195–207 (1999)
6. Floater, M.S.: Mean value coordinates. Comput. Aided Geom. Design **20**(1), 19–27 (2003)

7. Floater, M.S.: One-to-one piecewise linear mappings over triangulations. Math. Comput. **72**(242), 685–696 (2003)
8. Gaser, C., Dahnke, R., Thompson, P.M., Kurth, F., Luders, E., Initiative, A.D.N.: CAT-a computational anatomy toolbox for the analysis of structural MRI data. biorxiv, pp. 2022–06 (2022)
9. Jack, C.R., et al.: The Alzheimer's disease neuroimaging initiative (ADNI): MRI methods. J. Magn. Reson. Imaging **27**(4), 685–691 (2008)
10. Klein, A., Tourville, J.: 101 labeled brain images and a consistent human cortical labeling protocol. Front. Brain Imaging Methods **6**(171) (2012)
11. Kohavi, R., John, G.H.: Wrappers for feature subset selection. Artif. Intell. **97**(1–2), 273–324 (1997)
12. Kurtek, S., Srivastava, A., Klassen, E., Laga, H.: Landmark-guided elastic shape analysis of spherically-parameterized surfaces. Comput. Graphics Forum **32**(2), 429–438 (2013)
13. Pienaar, R., Fischl, B., Caviness, V., Makris, N., Grant, P.E.: A methodology for analyzing curvature in the developing brain from preterm to adult. Int. J. Imaging Syst. Technol. **18**(1), 42–68 (2008)
14. Razib, M., Lu, Z.L., Zeng, W.: Structural brain mapping. In: International Conference on Medical Image Computing and Computer Assisted Intervention (2015)
15. Reuter, M., Rosas, H., Fischl, B.: Highly accurate inverse consistent registration: a robust approach. Neuroimage **53**(4), 1181–1196 (2010)
16. Robinson, E.C., et al.: MSM: a new flexible framework for multimodal surface matching. Neuroimage **100**, 414–426 (2014)
17. Schoen, R., Yau, S.T.: Lectures on Harmonic Maps. International Press (1997)
18. Shattuck, D.W., et al.: Construction of a 3D probabilistic atlas of human cortical structures. NeuroImage **39**, 1064–1080 (2007)
19. Shi, R., et al.: Hyperbolic harmonic brain surface registration with curvature-based landmark matching. In: Gee, J.C., Joshi, S., Pohl, K.M., Wells, W.M., Zöllei, L. (eds.) IPMI 2013. LNCS, vol. 7917, pp. 159–170. Springer, Heidelberg (2013). https://doi.org/10.1007/978-3-642-38868-2_14
20. Smith, J., Schaefer, S.: Bijective parameterization with free boundaries. ACM Trans. Graphics **34**(4CD), 70.1-70.9 (2015)
21. Snoek, J., Larochelle, H., Adams, R.P.: Practical Bayesian optimization of machine learning algorithms. In: Advances in Neural Information Processing Systems, pp. 2951–2959 (2012)
22. Tsui, A., et al.: Globally optimal cortical surface matching with exact landmark correspondence. In: Gee, J.C., Joshi, S., Pohl, K.M., Wells, W.M., Zöllei, L. (eds.) IPMI 2013. LNCS, vol. 7917, pp. 487–498. Springer, Heidelberg (2013). https://doi.org/10.1007/978-3-642-38868-2_41
23. Yeo, B.T., Sabuncu, M.R., Vercauteren, T., Ayache, N., Fischl, B., Golland, P.: Spherical demons: fast diffeomorphic landmark-free surface registration. IEEE Trans. Med. Imaging **29**(3), 650–668 (2010)
24. Zeng, W., Yang, Y.-J.: Surface matching and registration by landmark curve-driven canonical quasiconformal mapping. In: Fleet, D., Pajdla, T., Schiele, B., Tuytelaars, T. (eds.) ECCV 2014. LNCS, vol. 8689, pp. 710–724. Springer, Cham (2014). https://doi.org/10.1007/978-3-319-10590-1_46